Residual Stress Modeling of Junction Structures Using Powder Injection Laser Cladding of Martensitic Stainless Steel on Low Alloyed Carbon Steel Substrate

Bita Mohajernia[1] and Jill Urbanic[2]

[1]University of Windsor, mohajerb@uwindsor.ca
[2]University of Windsor, jurbanic@uwindsor.ca

Corresponding author: Bita Mohajernia, mohajerb@uwindsor.ca

Abstract. Junction structures and rib constructions are utilized in various applications such as lightweight designs. As well as geometric challenges, using directed energy deposition metal additive manufacturing techniques to build intersections and junctions has the risk of having hydrostatic residual stress that can cause distortion or failure in the component. In this research, the residual stresses were measured computationally via a calibrated finite element analysis model for several junction structures, which the junction stresses evaluated as a function of deposition direction and order of operations. The path strategy significantly affects the mechanical and tensile properties of the junctions. This research needs to be extended to evaluate junctions for multi-layer scenarios.

Keywords: Laser cladding, Junction structure, Residual stress, Path strategy.
DOI: https://doi.org/10.14733/cadaps.2022.1070-1092

1 INTRODUCTION

Laser cladding is an additive manufacturing (AM) technique that is used broadly to coat surfaces, create new parts, or repair existing parts. It is one of the directed energy deposition (DED) AM processes. Laser cladding provides localized and relatively low heat input to produce a clad with ideal properties and minimal dilution with the substrate [1]. The use of laser cladding as an additive manufacturing process has been growing increasingly as it has many unique advantages over conventional cladding done through welding or metal deposition in terms of costs of materials, laser equipment, comparable rapid prototyping processes, and overall quality of the deposited materials [16]. Machine tool and robotic systems are platforms utilized for DED processes as opposed to dedicated enclosed systems [8]. These machine tool-based solutions can have large build envelopes, and can combine machining and additive manufacturing to allow for hybrid manufacturing strategies.

As with other AM processes, in laser cladding the 3D part is sliced into 2D layers and tool path strategies are developed to build the part. Unlike machining, the tool path strategy is an important factor for the mechanical properties and surface quality of the built part [4], [12], [2], [14]. For

bead deposition AM processes such as laser cladding, both the profile and the mechanical properties of the junctions are affected by the tool path deposition strategy.

During laser cladding, beads of material are placed side by side to create layers. The powder or wire feedstock material(s) are deposited and fused using laser power. Experimental data from prior research was used to develop a calibrated simulation model that was extended for this research. A powder feedstock was employed using a deposition head that delivered the powder and inert gas from the ducts around the laser nozzle. Either as a near net shape or as a final build, components with many pockets that are built from a DED AM process would employ significantly less material usage compared to machining from bar stock (Fig. 1). However, the cyclic rapid heating and solidification of the deposited material during the laser cladding process leads to the formation of residual stress, which results in the distortion of the part and the substrate. Generally, both tensile and compressive stresses could exist in the cladded materials. The presence of compressive stresses at the surface of the clad parts could improve its service life while the existence of tensile stresses could result in its premature failure through micro cracks. The type, magnitude, and locations of the residual stresses all influence the final component quality and service life.

(a) 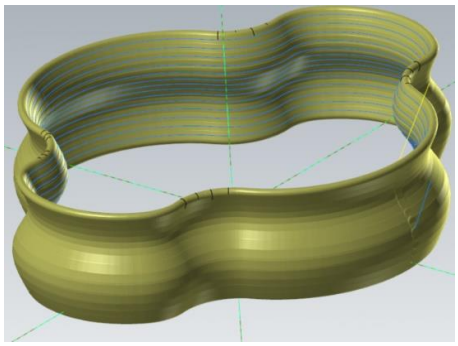 (b) 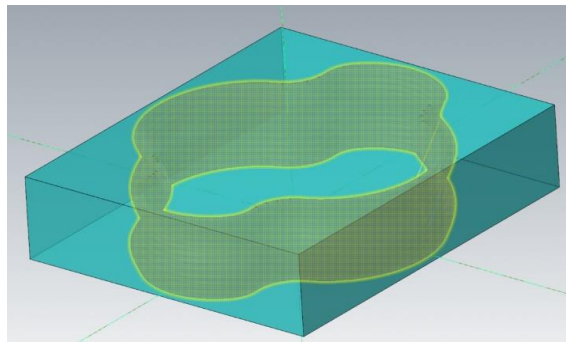

Figure 1: (a) Complex thin-walled shape, (b) bounding box illustrating the waste material (97%) for this component to be machined from stock.

Researchers have studied the effect of path planning strategies on different case studies from many aspects such as improving the geometrical or mechanical properties of the final part and proved it experimentally, however the experimental approaches are costly and limited scenarios can be assessed.

Shi et al. [15] proposed novel multi-node trajectory planning for fabricating grid stiffened panels. This resulted in a reduction of production time, energy and material waste, while simultaneously minimizing the number of interruptions. The procedure and the trajectory planning were validated experimentally. J.R Honnige et al. [4] investigated the effect of vertical inter-pass rolling and thermal stress relieving on Ti-6Al-4V intersections produced by wire + arc additive manufacturing. Thermal stress-relieving significantly reduced the residual stress in the intersection structure. Inter-pass rolling improved the grain refinement of the intersection. G. Venturini et al. [18] classified cross features into multiple types and used a single path deposition strategy via developed CAM software to create each structure with the aim of minimizing the geometrical errors. Han et al. [3] utilized three different scanning strategies to build samples and discovered that the flatness and surface roughness of a square-framed scanning strategy are better than those built from zig-zag patterns.

Ma et al. [7] proposed an adaptive path planning method that has varying thickness to successfully build thin-walled parts, and validate their method experimentally; however, they did not explore junction variants.

Nazemi et al. [11] did complementary research, exploring the computationally less expensive modeling techniques, to investigate the residual stress, distortion, and hardness in specimens with different deposition patterns. The rectangular specimens were built with longitudinal and transverse directions, as well as a spiral and fill-outward pattern. Comparing three different deposition patterns, it was concluded that the spiral outward and longitudinal patterns have the highest and lowest values of distortions, as well as the highest and lowest values of mean compressive and tensile residual stresses. Therefore, in tandem with addressing geometric issues, the path planning sequences are important, and research needs to be performed to explore tool path variants.

Jorn et al. [9] used finite element models to consider the thermo-mechanical performance of crossing structure deposited by wire arc additive manufacturing technique to overcome the issues related to accumulation of material or deposition failure when creating cross structures. The proposed deposition patterns had similar thermo mechanical performance.

Runsheng Li et al. [6] proposed a novel path strategy for intersections in wire arc additive manufacturing. Their proposed End Lateral Extension method eliminates the tightened defects at an intersection, and improved the tensile properties of junctions; however, only T junctions and structures consisting of three joints were assessed.

Much research work has been done on the performance of different path strategies for printing intersecting structures. The abovementioned studies suggested and applied different path strategies for cross structures. They mostly discussed the impact on the geometry and the profile. There are limited studies investigating the mechanical properties of intersections. Therefore, the goal of this research is to explore the influence of tool paths on the residual stresses. As material build up is an issue at intersections, novel 'design for DED' junction solutions are presented and discussed as well.

2 RESEARCH METHODOLOGY

The laser cladding research roadmap is shown in Fig. 2. This is a continuation of previous experimental and simulation studies.

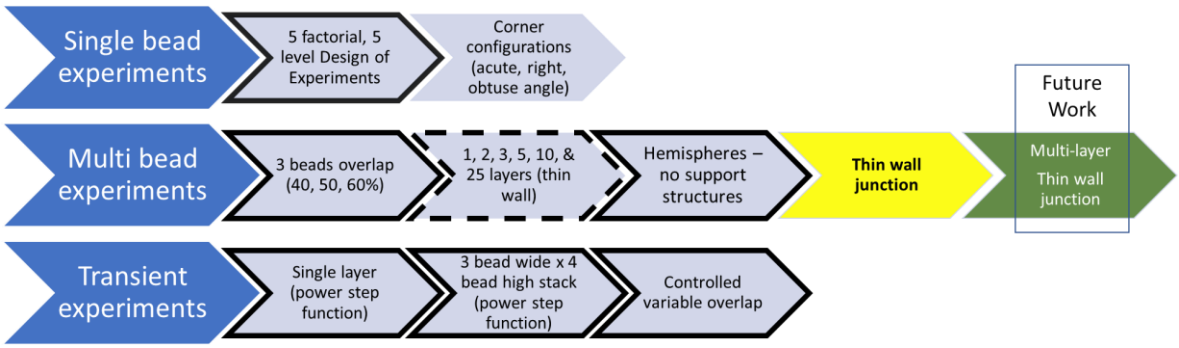

Figure 2: Experimental studies – blue & no border, experimental and simulation studies - blue & solid border, experimental and in-process simulation studies blue & dashed border, simulation studies – yellow (this research), green (future work) [13].

The first step for this research is to establish general problem sets for the various case studies and identify the process planning issues related to residual stress accumulation. Junction structures with three joints, four joints and five joints with a selection of possible different path deposition directions have been considered for this study as showed in Fig. 3. A path planning platform can be established

to help choosing the most appropriate deposition direction with respect to amount of residual stress formation in similar junction structures. A single path single layer deposition structure with constant wall thickness is considered for the junctions investigated in this work. The process parameters including heat source characteristics, laser velocity, the energy and the efficiency of the process are considered constant for all junction scenarios when setting up the thermo mechanical model [10], and are described in detail in the next section. The case studies being considered explore multiple time-temperature influences for differing operation orders. For the three junction sets, four configurations are modeled. The tool path direction is shown, and the order of operations are marked with numbers. The stop start-stop percentage overlaps are not considered for this research although not properly managing this issue introduces material stacking or poor bonding conditions.

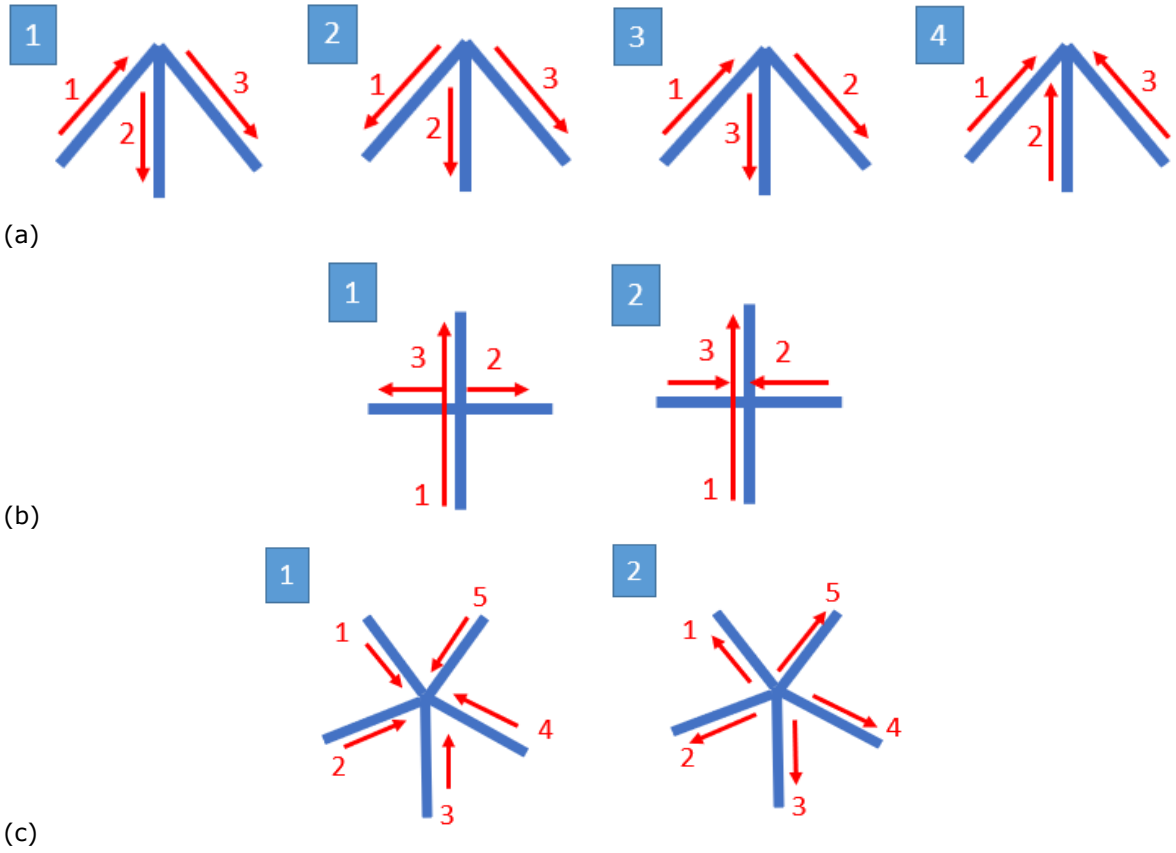

Figure 3: Junction structures and deposition sequential (a) Three joints, (b) Cross three joints, (c) Five joints.

These localized case studies can provide insights into the stress accumulations, but no component will consist of one junction type. In order to expand the effect of deposition direction on residual stress formation in junction structures, a modified three joint cross intersection and a hexagonal shape junction has been defined and studied. These case studies that are more similar to practical industrial application are shown in Fig. 4. The hexagon structure includes 2, 3 and 4 joint junctions' configurations within the same component. In these configurations, the residual stresses for two different sequence of deposition direction are compared for each case.

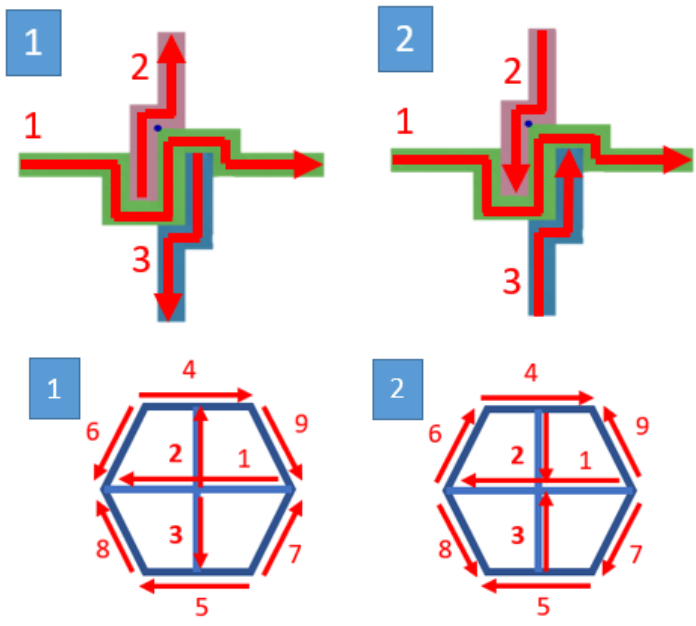

Figure 4: The deposition sequential in (a) Modified three joints junction, (b) Hexagonal shape junction.

Once the case studies were established, simulation models are created. The geometrical dimensions of the laser cladded specimens and substrates are demonstrated in Fig. 5. The plate thickness is constant for all scenarios 5 mm. The substrate sizes and bead lengths vary, but they are representative of larger components. A single bead, single layer of martensitic stainless steel X20Cr13 (similar to P410 and P420 stainless steel) deposited on a low alloyed carbon steel S355J2G3 (AI 1018) substrate. The bead and the substrate material have been studied and experimentally validated in previous research studies [11], [13], [10]. The single bead width and height are 4 mm and 1 mm respectively.

3 NUMERICAL SIMULATION AND RESULTS

Five unique junction case study families were considered, and numerical simulations were developed for each one incorporating different path scenarios. The single bead single layer deposition of martensitic stainless steel on low alloyed carbon steel is studied for each configuration. To model the laser cladding process, three software packages were used. The computer aided design software SOLIDWORKS was used to create the junctions' structure and the substrate. The created components were then imported into the HYPERMESH package to generate the appropriate mesh for the finite element analysis (FEA). A fine mesh using 8 node hexahedron solid elements were created for both the beads and the substrate. The 2D, 4 node elements were extracted from the 3D elements on the surface to dissipate heat via convection and radiation. The 1D 2 node elements that determine the welding path were created as well. Following generating the mesh the file was imported into the simulation software package, SYSWELD. A coupled thermal-metallurgical-mechanical analysis was performed. At first the transient heat transfer analysis takes place and the resulted temperature data are used as an input of the mechanical and metallurgical analysis. The temperature distribution at each node is extracted using the following equation (3.1) [11].

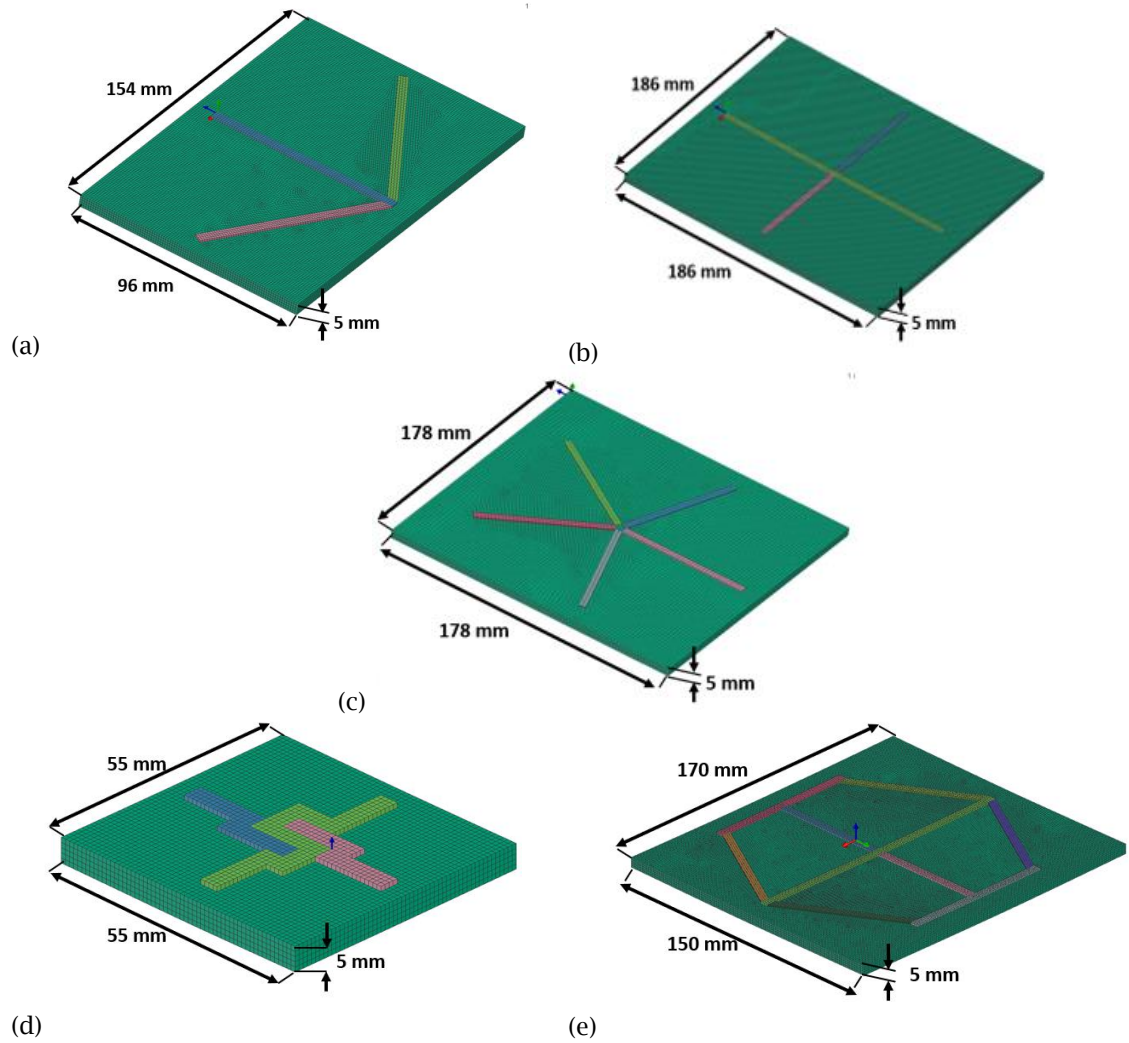

Figure 5: The geometrical dimensions of case studies (a) three joints, (b) four joints, (c) five joints, (d) modified three joints, (e) hexagon pattern with multiple junction structures.

$$\partial \frac{(\rho C_p T)}{\partial t} = \frac{\partial}{\partial x}(K\frac{\partial T}{\partial x}) + \frac{\partial}{\partial y}(K\frac{\partial T}{\partial y}) + \frac{\partial}{\partial z}(K\frac{\partial T}{\partial z}) + Q(x,y,z,t) \tag{3.1}$$

$\rho\ (\frac{Kg}{m^3})$ is the material density, $C_p\left(\frac{J}{Kg\ K}\right)$ is the specific heat capacity, $T\ (K)$ is the temperature, $K\ \left(\frac{J}{m\ K}\right)$ is the thermal conductivity, $Q\ \left(\frac{W}{m^2}\right)$ is the heat generation rate, $x, y\ and\ z$ are the nodes coordinates (mm) and $t(s)$ is the time.

The heat losses during laser cladding consisting two terms of convection and radiation are calculated by Newton's law and Stephan-Boltzmann's law respectively using the following formula:

$$q_{conv} + q_{rad} = h_C(T_s - T_0) - \varepsilon\sigma(T_s^4 - T_0^4) \tag{3.2}$$

h_C ($\frac{W}{m^2 K}$) is the heat convective coefficient, T_S is temperature of the surface, T_0 is the ambient temperature (20 ℃), ε is the emissivity of the surface and σ is the Stefan-Boltzmann's constant. The ambient temperature is considered for the primary temperature of the specimens and at the end of the process the models are cooled to the room temperature.

Using the SYSWELD software, the laser cladding scanning strategy was defined by selecting the start and stop points of laser movement within the bead and the substrate. This modeling approach uses a moving heat source to emulate the process. In order to simulate the laser cladding process a Gaussian heat source distribution was applied along the scanning path. The Gaussian heat source is demonstrated in Fig. 6 and defined by equations (3.3) to (3.5) [5].

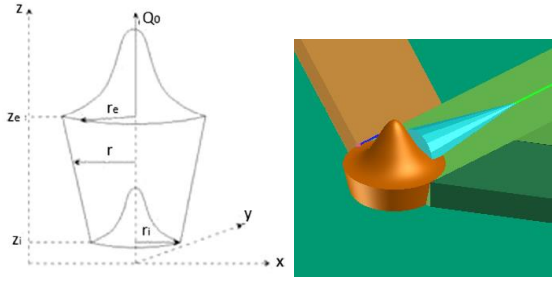

Figure 6: The Gaussian heat source schematic [5].

$$F = Q_0 * e^{\left(-\frac{r^2}{r_0^2}\right)} \tag{3.3}$$

$$r = (x^2 + y^2)^{1/2} \tag{3.4}$$

$$r_0 = r_e - (r_e - r_i) * (z_e - z)/(z_e - z_i) \tag{3.5}$$

F is the source intensity, Q_0 is the maximum source intensity, r_e is the keyhole top radius at $z=z_e$, and r_i is the keyhole bottom radius at $z = z_i$. The laser penetration depth was adjusted to 1.5 times of each layer. The parameters used in simulation are reported in Tab. 1. The process parameters and beads and substrate material are selected based on the calibrated model using experimental data [13].

Process parameter	Value
Heat source	beam
Velocity (mm/sec)	10
Energy (J/mm)	90
Efficiency (Percentage)	100

Table 1: Process parameters used in the simulation.

The substrate was clamped at four corners in the back plate using rigid boundary conditions. Succeeding the build process, the part is air cooled to the room temperature via convective, radiative heat transfer. The element activation and deactivation method were used in SYSWELD to model the layer-by-layer deposition of material. In this method all elements are generated prior to the simulation starting, however the elements are not activated until the laser beam reaches to that element. Moving the laser beam along the deposition direction, the elements become activated along the path.

The material properties of the substrate (a low alloyed carbon steel) and the beads (a martensitic stainless steel) as a function of temperature are defined in Fig. 7. These temperature dependent physical and mechanical data in the range of ambient to melting temperature are used as input data for the analysis. The plastic behavior of materials is assessed by the Johnson-Cook model. The input material properties used in the analysis were extracted form material database of the SYSWELD.

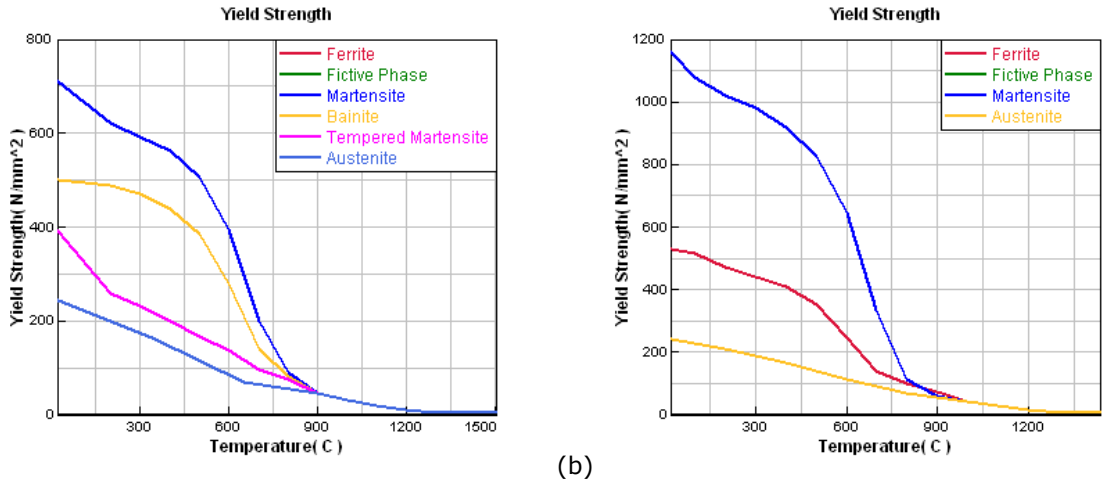

Figure 7: Yield strength of (a) low alloyed carbon steel WS355J2G3, (b) Martensitic stainless steel X20Cr13.

A baseline to compare residual stress results is established by selecting multiple points within the model scenarios for the different travel paths. A cross section of the cross-junction structure was taken at the center of the model (Fig. 8).

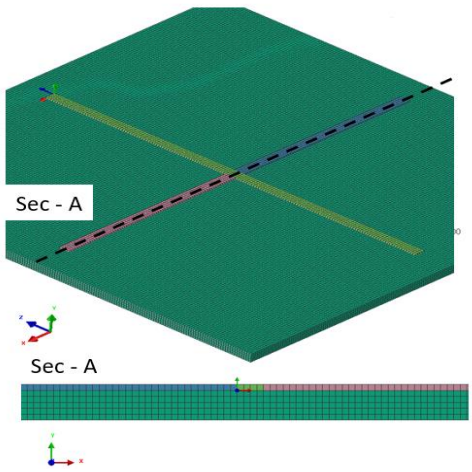

Figure 8: the cross section taken at the center of the specimen for the cross structure.

The schematic residual stress contour for the cross structure for these two different scenarios and plotted results for the two different build options are illustrated in Fig. 9. The residual stress measurement in the x direction was performed. The results are plotted through the bead thickness

for two different paths as prior experimental and simulation studies identified high tensile and compressive stress variations from the bead surface to the substrate interior, and that the magnitude of the stresses vary along the bead positions.

The path number one reference point is defined at the end of one bead in the first scenario. This location is the start of the bead for the second scenario. The second path reference point was considered at a point in the center of the structure. The measurements are performed from the top of the bead through the substrate region. Therefore, the maximum distance to be considered for the data analyses is 6 mm.

For the x direction, the range of residual stresses varies from 708 MPa to -514 MPa for this data set. Fig. 9 shows the cross section considered and the colour map clearly illustrates the residual stress variations at any cross section and along the bead. Fig. 9 (a) and 9(b) shows the node points analyzed and the distinct residual stress differences at these points for version one and two respectively.

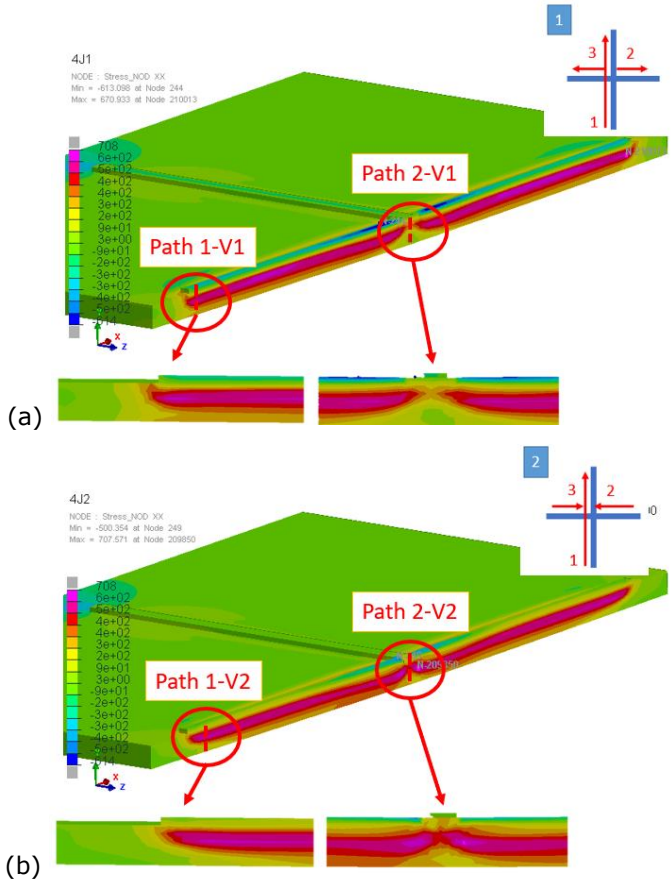

Figure 9: The residual stress measurement for two different paths through the depth (a) The first scenario and (b) the second scenario.

The stress-distance diagram is plotted using the residual stress values at each node through the depth for two predefined paths as is illustrated in Fig. 10.

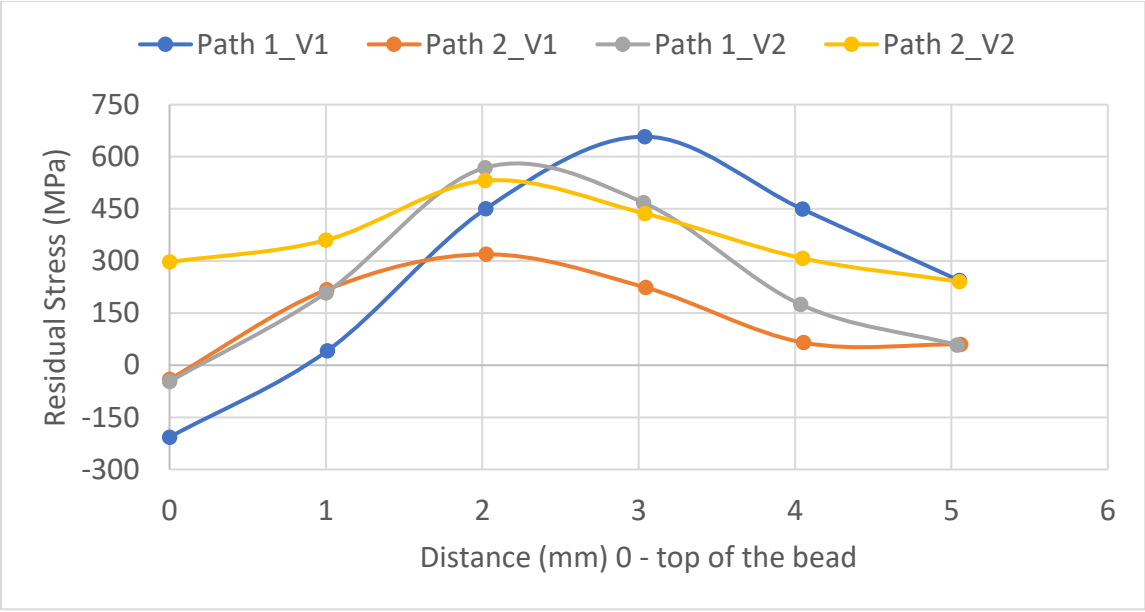

Figure 10: The 4-junction stress (MPa)-distance (mm) diagram for two different paths in two scenarios V1 and V2.

The maximum amount of residual stresses are tensile stresses for this data set. The stresses are noticeably higher for the second scenario; however, the compressive residual stresses are less in the first scenario. It can be seen that in the center of the structure in the second scenario, the amount of residual stresses is higher due to the deposition direction of the second and third bead (radiate inward). This indicates that directional control is important for process planning software design, and for process planners. The tensile residual stresses close to the edge of the beads were stabled by the compressive residual stresses formed toward the edges as demonstrated in residual stress contour plot. Locational variations are important to understand, as this may introduce the need for laser only tool paths to modify the material structures. No stress patterns can be determined at the top of the beads. The largest values of compressive and tensile residual stresses occur with the V1 option (and the range is 864 MPa); whereas, low magnitude compressive stresses occur for the V2 option (-40 to -46 MPa). When plotting the results for the two junction variants, three data sets have a peak tensile stress within the component at the 2 mm point, or 1 mm into the plate. The peak tensile stresses vary from 319 to 657 MPa. The compressive stresses vary between -207 MPa (Path 1_V1 start) to -40 MPa (Path 2_V1 start). The Path 1_V1 results indicate a peak tensile stress value at 3 mm (2 mm into the plate).

The residual stress contours in the YY and ZZ direction are shown in Fig. 11. The magnitude of the tensile and compressive stresses in the YY direction for version one is in the range -412 to 237 (MPa) and for version two varies from -518 to 246 (MPa). For the ZZ direction these residual stress values vary from -875 to 653 MPa for version one and from -577 to 643 MPa for version two. A comprehensive comparison analysis will be performed using the methodology developed by Urbanic et al. in 2019 [17].

A section cut of the modified junction structure that was considered is shown in Fig. 12. This cross section captures all three beads, and two distinct variants for the continuous bead.

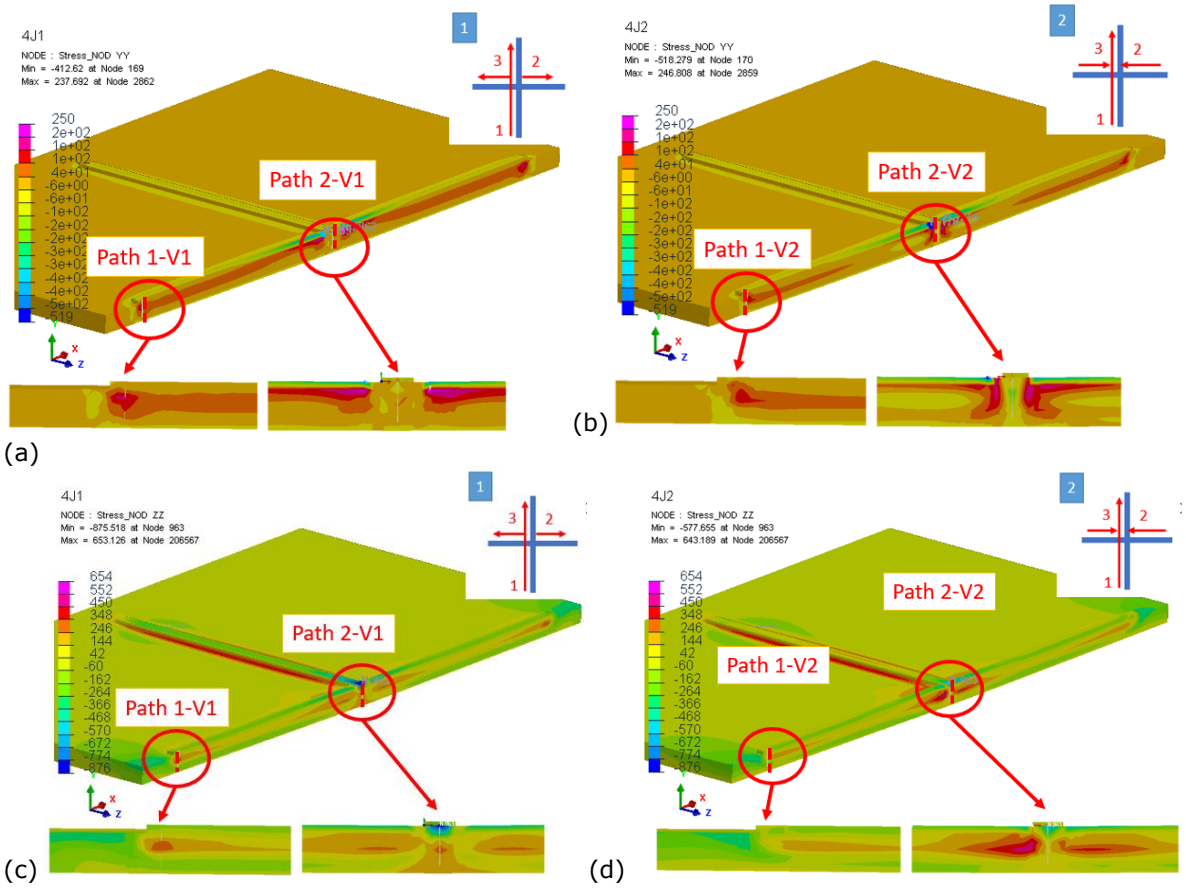

Figure 11: The residual stress contour: (a)σyy, first scenario, (b) σyy, second scenario, (c) σzz, first scenario, (d) σzz, second scenario.

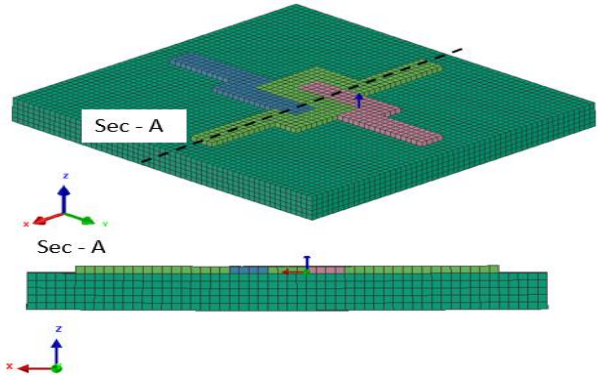

Figure 12: the cross section taken at the center of the specimen for the modified junction structure.

Fig. 13 shows the color map for the considered cross sections in the modified junction structure. Fig. 13 (a) and 13(b) shows the node points analyzed and the distinct residual stress differences at these points for the first and second scenario, respectively.

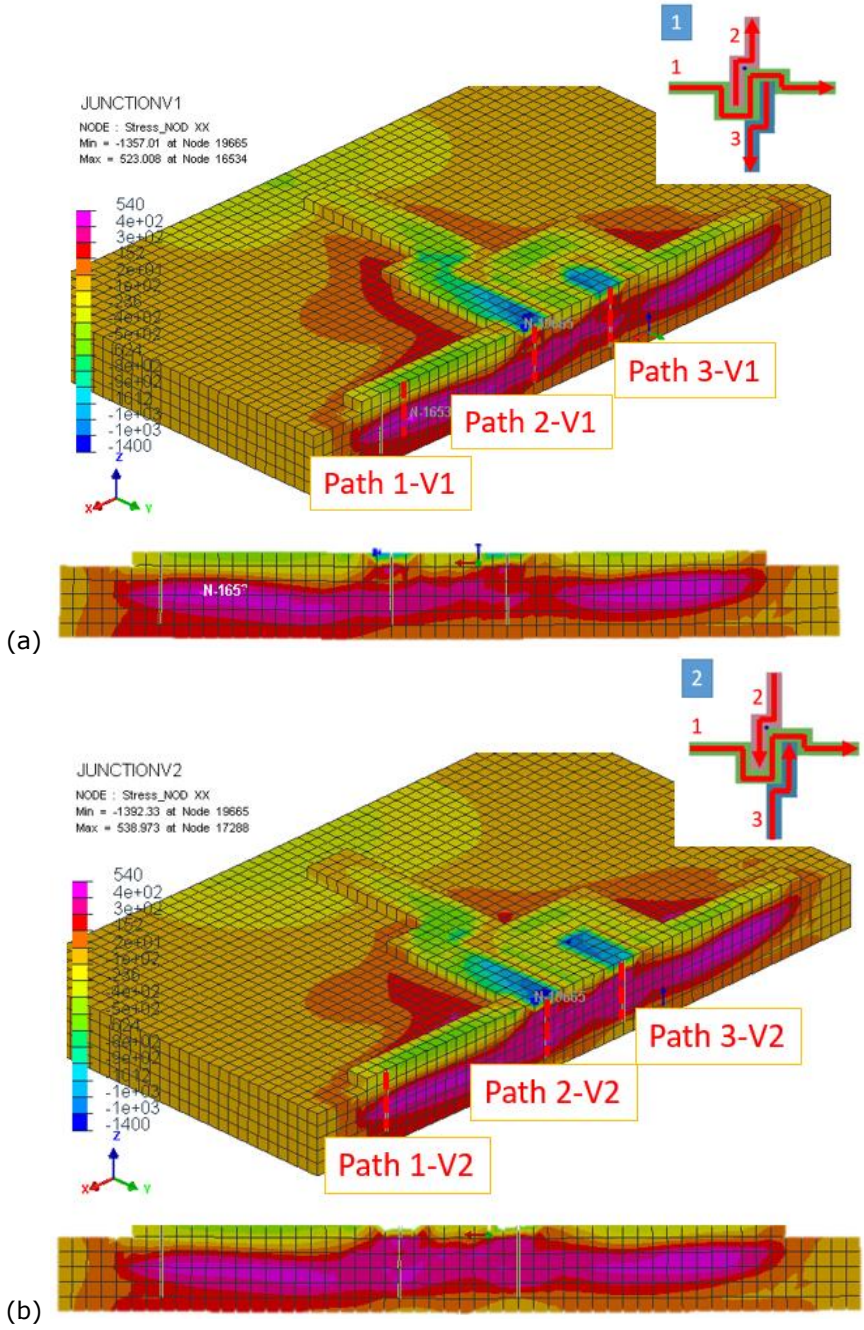

Figure 13: The residual stress measurement for three different paths through the depth (a) The first scenario and (b) the second scenario.

The stress-distance diagram is plotted using the residual stress values at each node through the depth for three predefined paths as is illustrated in Fig. 14. Compressive residual stresses occur at the top of all the beads with the V1 and V2 options for the modified junction bead geometry and two distinctive residual patterns can be extracted from this data set.

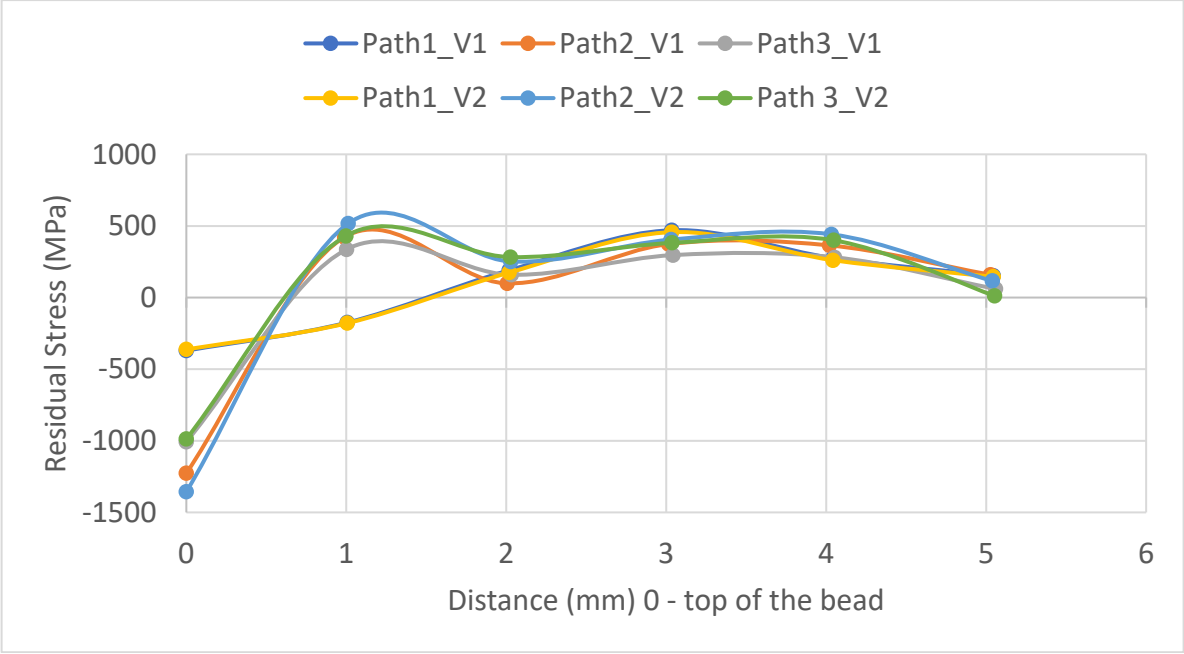

Figure 14: The modified junction stress (MPa)-distance (mm) diagram for the three different paths and the two deposition scenarios V1 and V2.

The first path residual stress patterns and the observed magnitudes for both solution approaches are very similar, and it is difficult to extinguish any key differences. As with the Path1 results, the peak tensile stresses occur at the 3 mm measurement point (2 mm into the plate). The range of residual stresses are 841 and 819 MPa for the V1 and V2 scenarios, respectively. On average, the magnitudes vary by +/- 4% or 10 MPa for all data collection points. The subsequent travel paths all exhibit the same patterns, with compressive stresses at the bead surface, and data that oscillates in the tensile stresses' region. The overall range of residual stress values are high for the Path 2 and Path 3 results, and the stress results range from 1344 to 1872 MPa, which is approximately 1.5 to 2.2 times greater than the results generated with the four-junction solution. Excluding the first reference point at the surface, the average standard deviation is 58 MPa. Variations exist, but the average range is within 160 MPa. The curves appear to be a damped '2nd order' curve. This phenomenon may be something to explore in future studies.

The residual stress contours for the YY and ZZ direction are showed in Fig. 15. The magnitude of the tensile and compressive stresses in YY direction for version one is in the range -1373 to 585 (MPa) and for version two varies from -1483 to 609 (MPa). For the ZZ direction these residual stress values vary from -989 to 500 MPa for version one and from -1026 to 490 MPa for version two. The σ_{ZZ} maximum and minimum values for version one and version two are close to each other. This shows that the deposition sequence does not significantly affect the residual stress variation in Z direction for the modified junction structure.

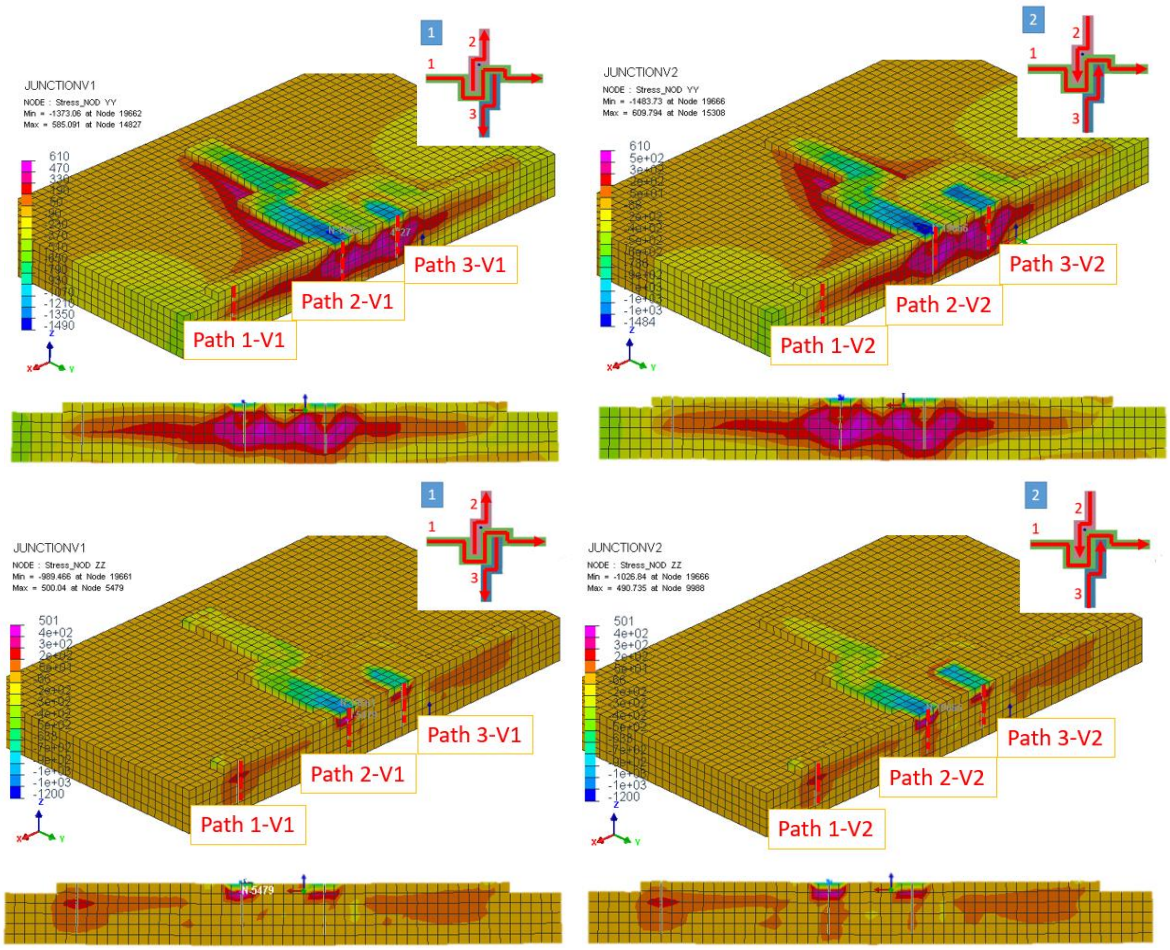

Figure 15: The residual stress contour: (a) σyy, first scenario, (b) σyy, second scenario, (c) σzz, first scenario, (d) σzz, second scenario

4 DISCUSSION

From the thermo-mechanical finite element analysis of various laser cladding process junctions and the differing tool path options, the sensitivities to the operation order and junction configuration are evident. The FEA simulations for this research focused on residual stresses, and the variations related to the deposition patterns are significant. This indicates that this knowledge needs to be captured and incorporated into DED AM process planning software as well as to process planners. There are 2^n pattern variants where n is the number of arms for a junction. This research indicates that more scenarios need to be explored to identify sensitivities. The minimum and maximum residual stresses for the 3, 4, and 5 junction sets analyzed in this work are compared in Fig. 16, 17 and 18.

In Fig. 16, the V1 build strategy has noticeably higher stresses; whereas, the other variants have relatively consistent maximum σxx and σzz tensile and compressive stress values. The σyy are significantly lower, especially for the V2 and V3 build scenarios. The 'radial in' has the next highest residual stress values. The 'radial out' scenario (V2) resulted in the best residual stress conditions. The V1 build approach introduces high σyy stresses, especially for the tensile residual stresses (Fig. 16).

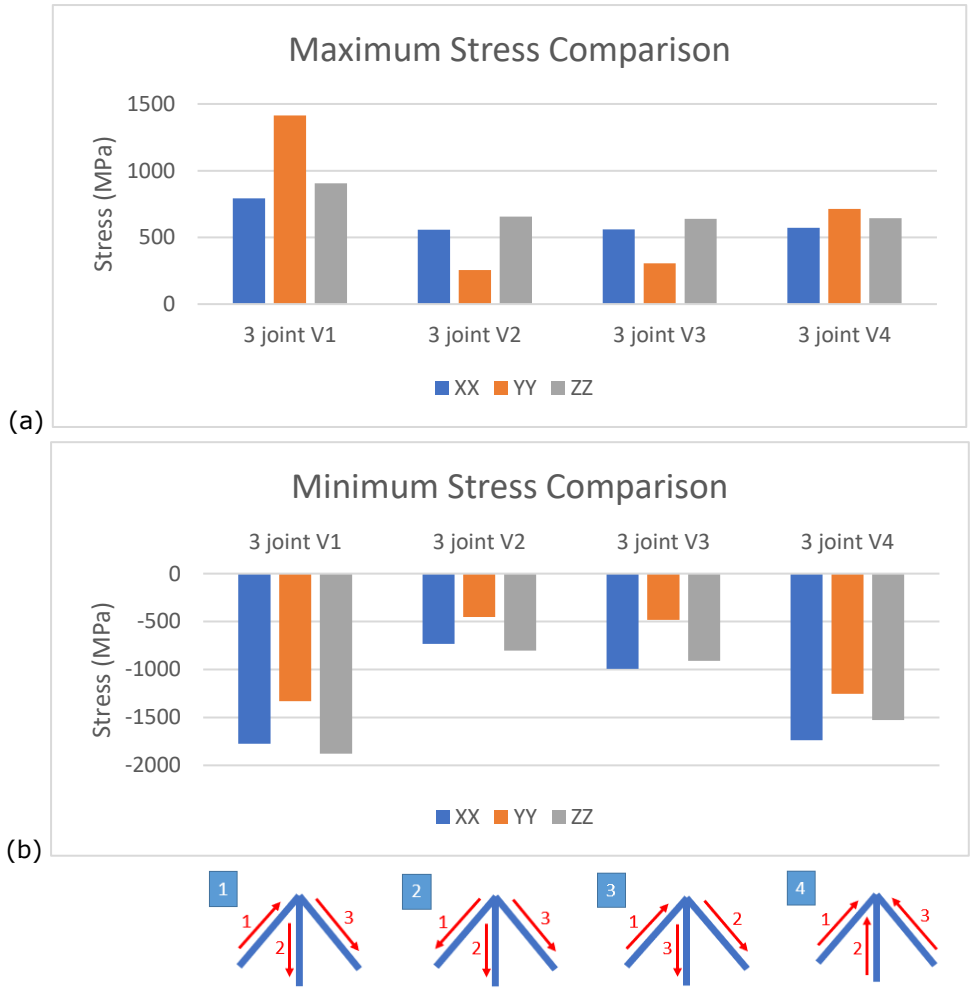

Figure 16: (a) A comparison of the maximum and (b) minimum stresses in the major planes for the 3 joint build scenarios.

Interestingly, the four-junction configuration has very similar results for both build options, and the magnitude of the observed stresses are similar to those from the 3 joint V2 build scenario. This can be seen in Fig. 17, where the four joint cross configuration is compared to best and worst cases for the three joint junction build approaches. The σyy values have the lowest magnitudes for both the tensile and compressive residual stresses.

The five junction scenarios, have similar results to the three junction V2 variant as well. This is shown graphically in Fig. 18. More variations for the σyy values can be observed, but they are still lower than the σxx and σzz values. The modified joint residual stress data are compared graphically to the four joint cross scenarios (Fig. 19). The modified joint has less σxx and σzz tensile stresses than the cross option (20% and 25.5% respectively), but the σyy stresses are noticeably higher (approximately 2.5 times higher). The compressive residual stresses are significantly higher for the modified joint junction. The V1 option is slightly better than the V2 option. The V1 option is a 'radial out' variant; therefore, this result is not unexpected.

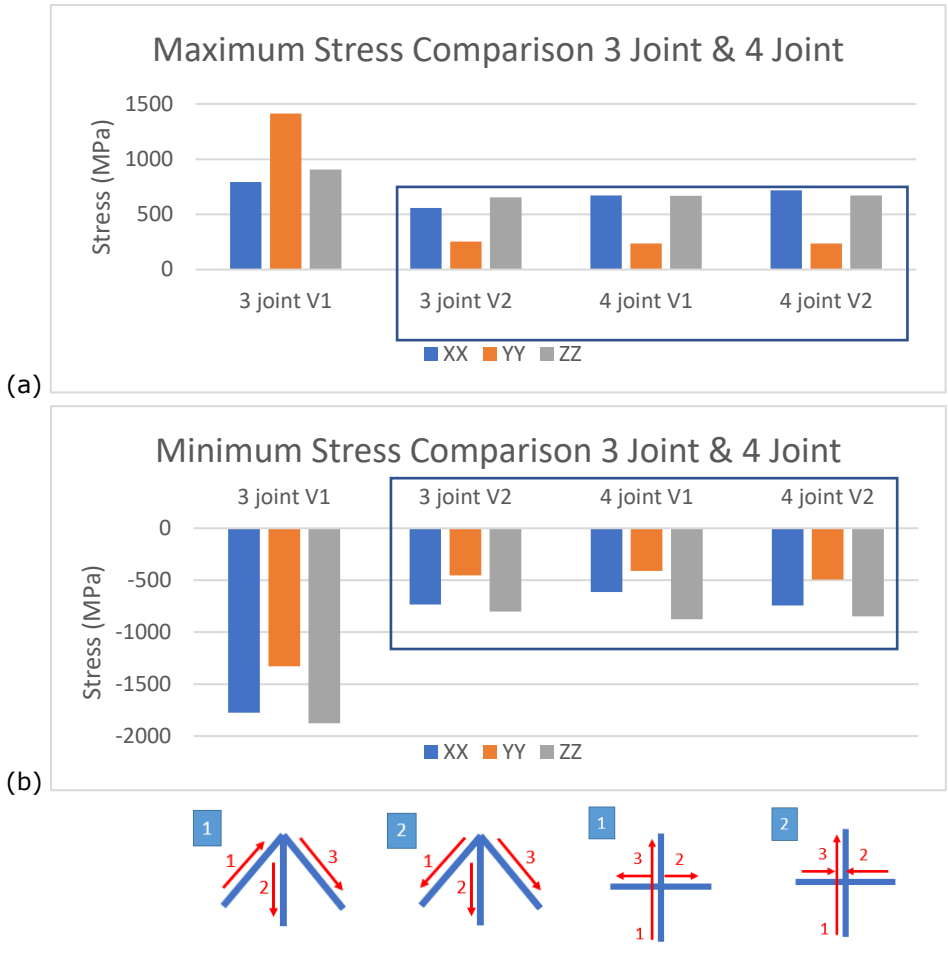

Figure 17: (a) A comparison of the maximum and (b) minimum stresses in the major planes for the extreme 3 joint build scenarios compared to the 4 joint cross scenarios.

None of these build options can be considered piecemeal. A realistic component will have multiple junctions, and no one solution can be utilized. The example in Fig. 3 (b) has two, three, and four junction sets. The magnitudes for the σxx, σyy and σzz values are very close to each other, and again are similar to the three joints V2 build option (Fig. 20).

The high compressive stress values for the Hex_V1 occur in a 'radial in' pattern, which is similar to the three joint V4 case, and is a condition to be avoided per the initial case study set. Although significantly more heat has been applied into the substrate for the hexagonal model case study, the results indicate this is a not an ideal build approach. As a comparison, the 'radiate out' condition (V2 vertex 9-1-7) has one third the compressive stresses.

The residual stress in the xx direction for a single path at the center of the joints for the 3-bead scenario was compared with the similar spot in hexagon junction as demonstrated in Fig. 21. The amount of residual stress starting from the bead surface through the depth of substrate was plotted. It was observed that in the second scenario of the hexagon junction in the marked area in Fig. 22 that the amount of residual stress is noticeably lower in comparison with the marked area of the first hexagon scenario.

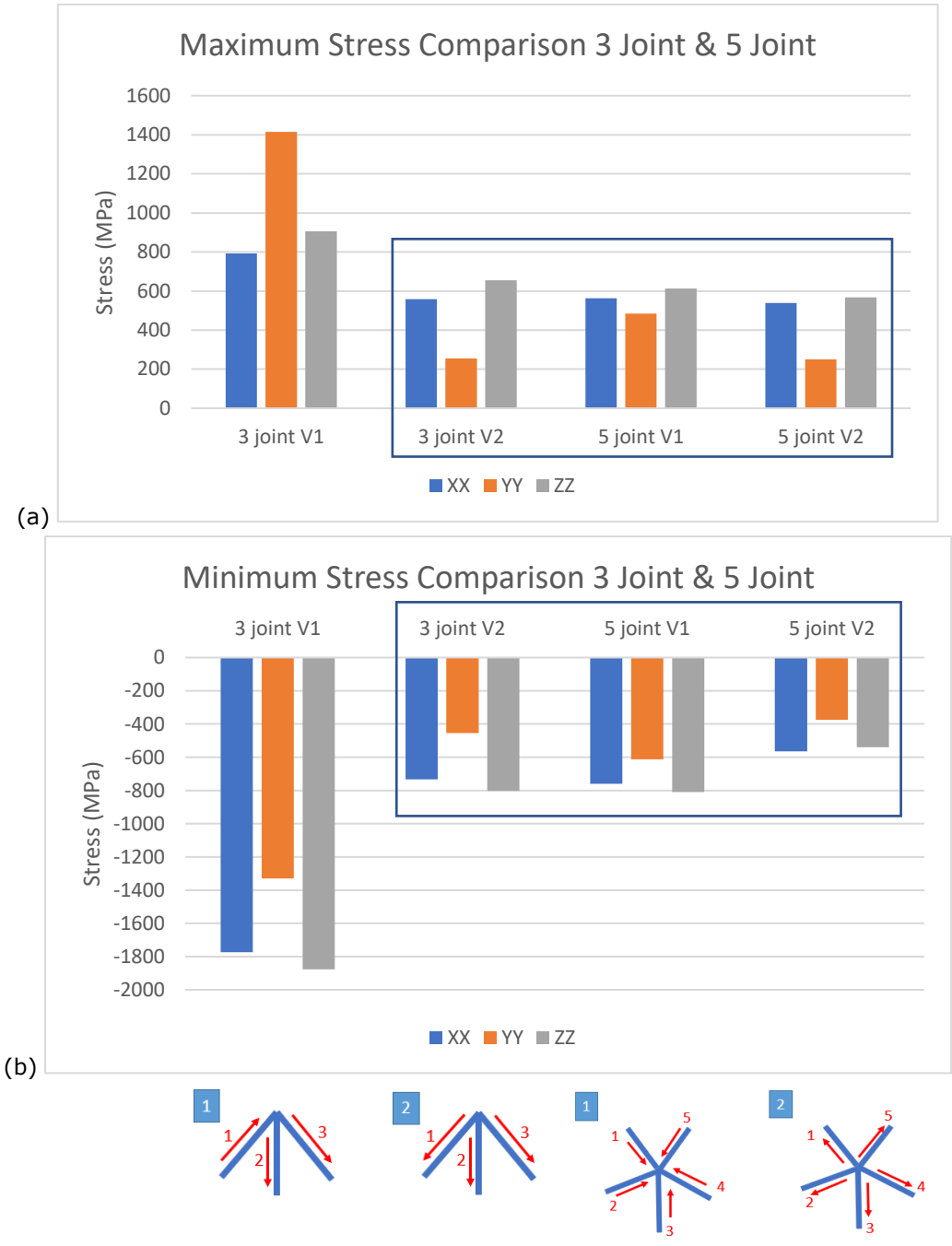

Figure 18: (a) A comparison of the maximum and (b) minimum stresses in the major planes for the 3 joint and 5 joint build scenarios.

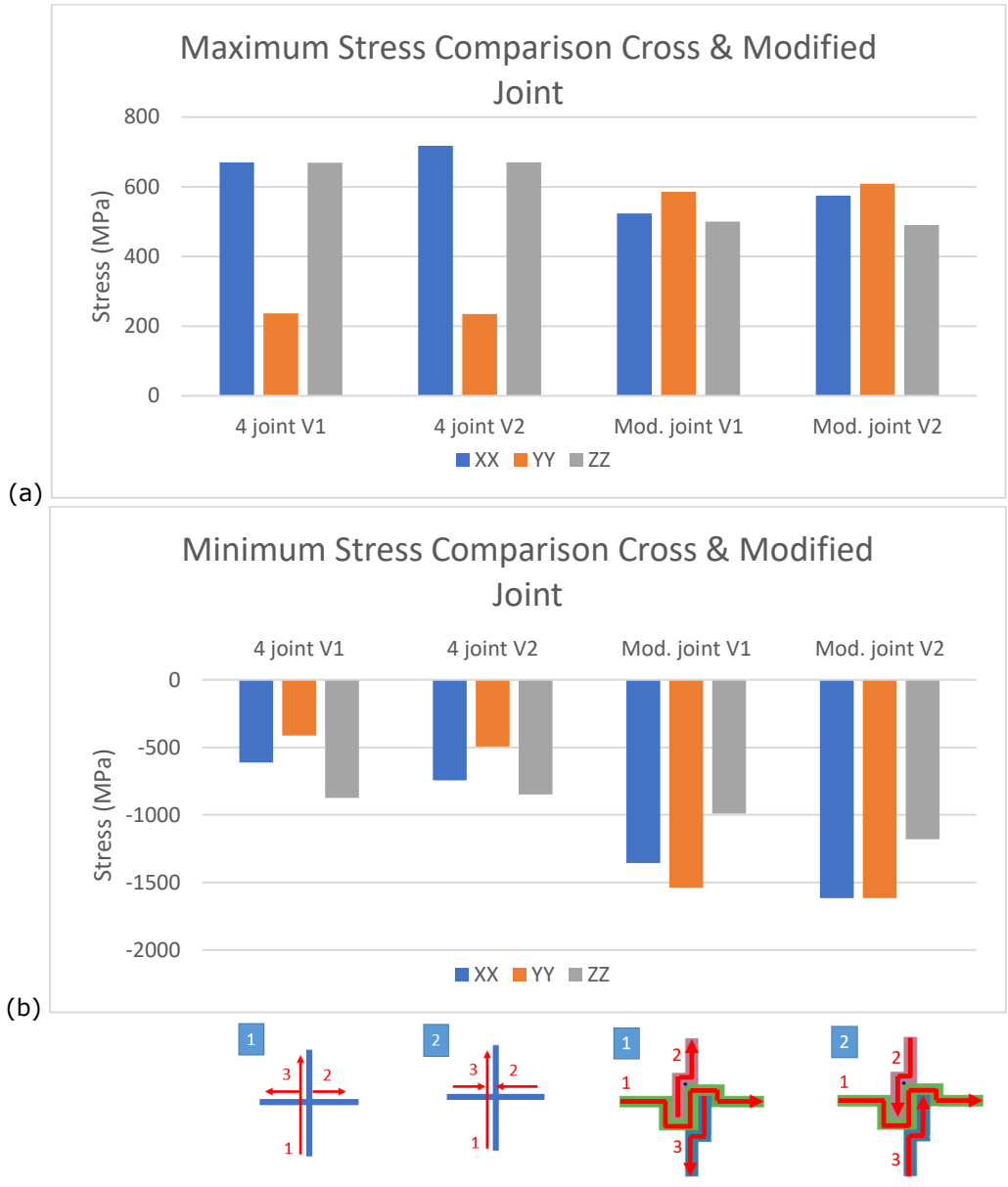

Figure 19: (a) A comparison of the maximum and (b) minimum stresses in the major planes for the 4 joint (cross) and the modified cross joint build scenarios.

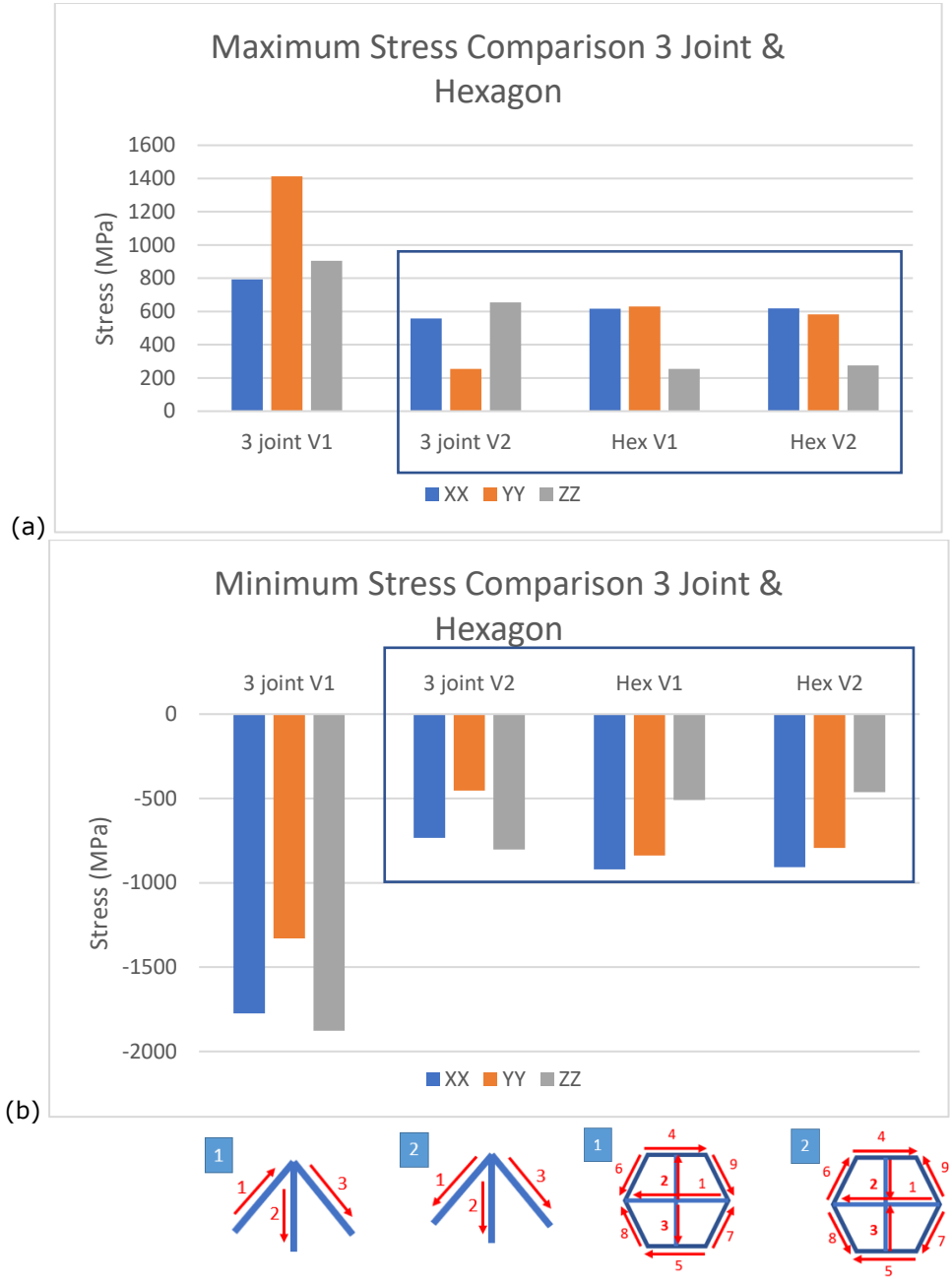

Figure 20: (a) A comparison of the maximum and (b) minimum stresses in the major planes for the 3 joint cases and the hexagonal model case study.

This is the trend to what we had for the three joints junction structure, considerably less amount of residual stress for the second scenario in comparison with the fourth one. It can be concluded that the inward deposition direction during the process will lead to formation of high residual stresses

and should be avoided as much as possible. At the 4 mm point, all data sets have the residual stress values converging to 0 MPa.

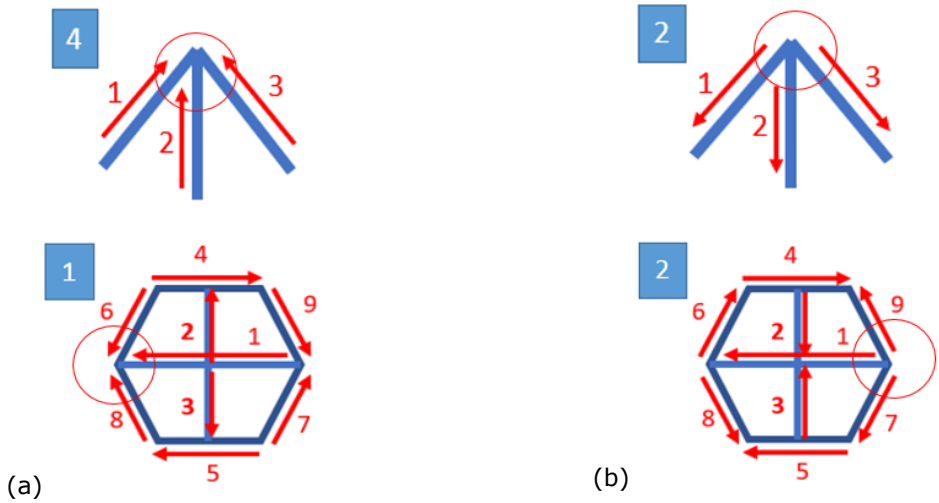

Figure 21: The location considered for results comparison, (a) Fourth scenario of the 3-joints junction being compared with first scenario of the hexagon, (b) Second scenario of the 3-joints junction being compared with second scenario of the hexagon.

Balancing the tool path order of operations needs to be performed for determining the best build options, but it appears that joints that connect four or five links have relatively similar results. Multiple case studies indicate a 'radial out' build strategy for a joint is preferred to reduce residual stresses. The challenge is to introduce a physically realizable build approach. Multiple layers and heat only pass need to be explored to determine whether the residual stresses can be minimized. The modified joint solution is physically realizable and introduces a mechanical joint at each junction, but the compressive residual stresses are significantly increased. This can be due to the mass of the material at the joint or the dimensions of the sample being analysed. A sensitivity study with respect to dimensions, bead widths and heights, and different mechanical joint shapes to shorten or lengthen the 'steps' will be explored.

Only the maximum and minimum stress values are assessed. It is important to compare the stress patterns, and the residual stress characteristics throughout the beads, not just at select points. Machine learning algorithms are being explored to complement the FEA analyses, as this method may allow comprehensive comparisons as well as predictions to be performed.

CONCLUSIONS

Residual stresses induced by the rapid heat cycling inherent in the laser cladding process were investigated for junction structures. Laser cladding is a DED process, and this process family lends itself to fabricating thin-walled components with pockets or junctions. There are geometric challenges with ensuring that there are proper overlapping solutions at intersection points, but these must be developed with tool path 'order of operations' and direction strategies. There are many alternatives to explore; therefore, thermo mechanical simulations were developed using FEA method to assess the effect of deposition direction and operation order on the formation of residual stress in junction structures. The following conclusions can be achieved from this study:

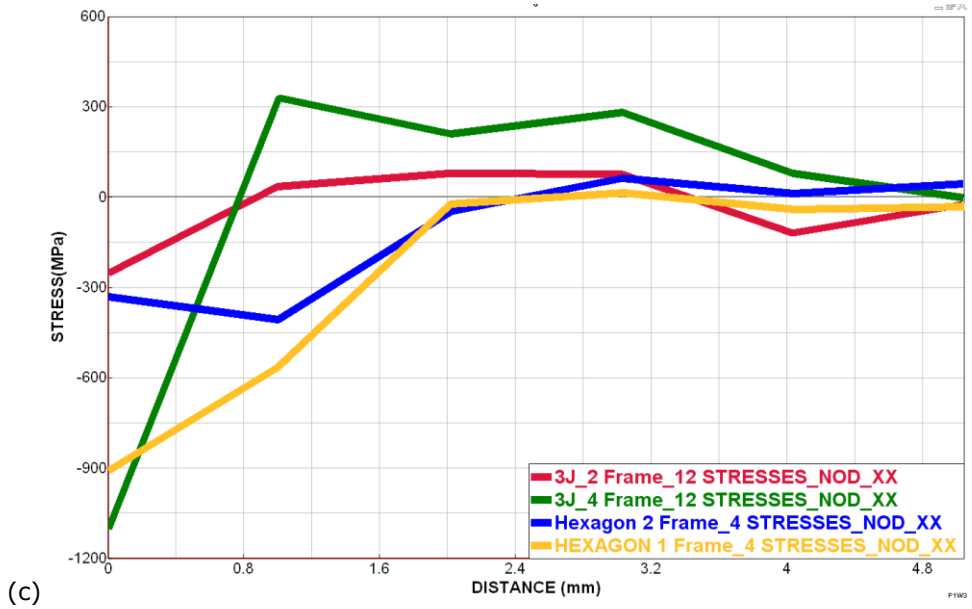

(c)

Figure 22: The residual stress curves for the selected points and build scenarios.

- Tensile residual stresses were observed close to the base plate and compressive residual stresses in the beads of the junctions for all junction configurations.
- The tensile residual stresses in the x, y and z directions for the first scenario in the three joint junction structure have the most extreme values compared to the other scenarios. This deposition solution could lead to performance issues in the field.
- Both deposition direction options for the cross structure showed nearly similar thermo mechanical performance; therefore, the configuration is less problematic.
- The first scenario of the five joints junction had the greatest amount of residual stress.
- The amount of the tensile residual stress in the modified three joint structure has decreased in comparison with the cross structure, however the compressive stress in the bead surface has increased. It should be noted that the substrate width and height in the modified junction are smaller when compared to the cross-structure scenarios. A sensitivity analysis will be performed to determine the influence factors.
- The first build scenario of the hexagon structure is worse in terms of overall residual stress characteristics; however, the trends observed for the individual case study analyses are consistent with this more realistic case study.

This study clearly illustrates the influence of the AM tool path strategy when considering performance criteria, and that AM CAD/CAM software must consider developing and managing tools to assist process planners with creating effective build operation lists. There are significant challenges to managing both the geometry and residual stresses, as localized high stress areas can result with a component consisting of multiple junctions. There are numerous potential build combinations to consider, and realistic case studies require multi-layer simulations. This is an ongoing area of research.

REFERENCES

[1] Chen, J.; Wang, S. H.; Xue, L.: On the Development of Microstructures and Residual Stresses during Laser Cladding and Post-Heat Treatments, Journal of Materials Science 2012, 47 (2), 779–792. https://doi.org/10.1007/s10853-011-5854-4.

[2] Bates, J.; Ding, M.-S.; Park, J.: A Study on Rapid Prototyping Techniques, TR UMCP-97-003, University of Massachusetts, Boston, MA, 1997, http://www.um.edu/~bates.html.

[3] Fu, J.; Qiu, K.; Gong, L.; Liu, C.; Wu, Q.; Lu, J.; Fan, H.: Effect of Tool-Path on Morphology and Mechanical Properties of Ti-6Al-4V Fabricated by Wire and Arc Additive Manufacturing, In MATEC Web of Conferences; 2017; Vol. 128, p 5009. https://doi.org/10.1051/matecconf/201712805009

[4] Eaton, J. A.: Layered Manufacturing Methods for Reconstructing Bone Structures, Ph.D. Thesis, University of Minnesota, Twin Cities, MN, 1998.

[5] Han, J.; Ge, Y.; Mao, Y.; Wu, M.: A Study on the Surface Quality of the 3D Printed Parts Caused by the Scanning Strategy, Rapid Prototyping Journal 2019. http://dx.doi.org/10.1108/RPJ-06-2017-0125

[6] Hönnige, J. R.: Control of Residual Stress, Distortion and Mechanical Properties in WAAM Ti64 Parts, 2017, 1–38. https://doi.org/10.4324/9781315545912.

[7] Kemerling, B.; Lippold, J. C.; Fancher, C. M.; Bunn, J.: Residual Stress Evaluation of Components Produced via Direct Metal Laser Sintering, Welding in the World 2018, 62 (3), 663–674. https://doi.org/10.1007/s40194-018-0572-z

[8] Li, R.; Zhang, H.; Dai, F.; Huang, C.; Wang, G.: End Lateral Extension Path Strategy for Intersection in Wire and Arc Additive Manufactured 2319 Aluminum Alloy, Rapid Prototyping Journal 2019. http://dx.doi.org/10.1108/RPJ-05-2019-0123

[9] Ma, G.; Zhao, G.; Li, Z.; Xiao, W.: A Path Planning Method for Robotic Wire and Arc Additive Manufacturing of Thin-Walled Structures with Varying Thickness, In IOP Conference Series: Materials Science and Engineering; 2019; Vol. 470, p 12018. doi:10.1088/1757-899X/470/1/012018

[10] Mazak, Integrex Multi-Tasking | Mazak UK. (n.d.) https://www.mazakeu.co.uk/machines-technology/by-product/integrex-multi-tasking/.

[11] Mehnen, J.; Ding, J.; Lockett, H.; Kazanas, P.: Design Study for Wire and Arc Additive Manufacture, International Journal of Product Development 20 2014, 19 (1–3), 2–20. https://www.researchgate.net/deref/http%3A%2F%2Fdx.doi.org%2F10.1504%2FIJPD.2014

[12] Mohajernia, B.; Urbanic, R. J.; Nazemi, N.: Predictive Modelling of Residual Stresses for Single Bead P420 Laser Cladding onto an AISI 1018 Substrate, IFAC-Papers OnLine 2019, 52 (10), 236–241. https://doi-org.ledproxy2.uwindsor.ca/10.1016/j.ifacol.2019.10.070

[13] Nazemi, N.; Urbanic, R. J.: A Numerical Investigation for Alternative Toolpath Deposition Solutions for Surface Cladding of Stainless Steel P420 Powder on AISI 1018 Steel Substrate, The International Journal of Advanced Manufacturing Technology 2018, 96 (9), 4123–4143. https://doi.org/10.1007/s00170-018-1840-1

[14] Nazemi, N.; Urbanic, R. J.: A Numerical Analysis Approach to Evaluate Hardness and Distortion for Selected Multi-Track Laser Cladding Configurations: P420 Steel Bead Deposition on Mild Steel, In ASME International Mechanical Engineering Congress and Exposition; 2017; Vol. 58356, p V002T02A023. https://doi-org.ledproxy2.uwindsor.ca/10.1115/IMECE2017-70618

[15] Nazemi, N.; Urbanic, J.; Alam, M.: Hardness and Residual Stress Modeling of Powder Injection Laser Cladding of P420 Coating on AISI 1018 Substrate, The International Journal of Advanced Manufacturing Technology 2017, 93 (9), 3485–3503. DOI 10.1007/s00170-017- 0760-9

[16] Ren, K.; Chew, Y.; Fuh, J. Y. H.; Zhang, Y. F.; Bi, G. J.: Thermo-Mechanical Analyses for Optimized Path Planning in Laser Aided Additive Manufacturing Processes, Materials and Design 2019, 162, 80–93. https://doi.org/10.1016/j.matdes.2018.11.014.

[17] Shi, J.; Li, F.; Chen, S.; Zhao, Y.: T-GMAW Based Novel Multi-Node Trajectory Planning for Fabricating Grid Stiffened Panels, An Efficient Production Technology. Journal of Cleaner Production 2019, 238, 117919. https://doi.org/10.1016/j.jclepro.2019.117919

[18] Telasang, G.; Majumdar, J. D.; Wasekar, N.; Padmanabham, G.; Manna, I.: Microstructure and Mechanical Properties of Laser Clad and Post-Cladding Tempered AISI H13 Tool Steel, Metallurgical and Materials Transactions A 2015, 46 (5), 2309–2321. DOI: 10.1007/s11661-015-2757-z

[19] Urbanic, R. J.; Mohajernia, B.; Nazemi, N.: Developing Geometric Analysis Tools to Compare Heat Map Results for Metal Additive Manufactured Components, Computer Aided Des Appl 2019, 17 (2), 288–311. https://www.researchgate.net/deref/http%3A%2F%2Fdx.doi.org%2F10.14733%2Fcadaps.2

[20] Venturini, G.; Montevecchi, F.; Bandini, F.; Scippa, A.; Campatelli, G.: Feature Based Three Axes Computer Aided Manufacturing Software for Wire Arc Additive Manufacturing Dedicated to Thin-Walled Components, Additive Manufacturing 2018, 22, 643–657. https://doi.org/10.1016/j.addma.2018.06.013